INTERNATIONAL JOURNAL OF HYDROGEN ENERGY XXX (2012) 1–11

Available online at www.sciencedirect.com

SciVerse ScienceDirect

journal homepage: www.elsevier.com/locate/he

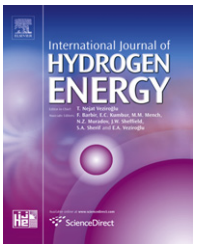

Nonlinear stability analysis and a new design methodology for a PEM fuel cell fed DC–DC boost converter

Damian Giaouris [a,b,*], *Fotis Stergiopoulos* [b,c], *Chrysovalantou Ziogou* [b], *Dimitris Ipsakis* [b], *Soumitro Banerjee* [d], *Bashar Zahawi* [a], *Volker Pickert* [a], *Spyros Voutetakis* [b], *Simira Papadopoulou* [b,c]

[a] *School of Electrical and Electronic Engineering, Newcastle University, Newcastle upon Tyne NE1-7RU, UK*

[b] *Chemical Process Engineering Research Institute (C.P.E.R.I.), Centre for Research and Technology Hellas (CE.R.T.H.), P.O. Box 60361, 57001 Thermi-Thessaloniki, Greece*

[c] *Department of Automation, Alexander Technological Educational Institute of Thessaloniki, P.O. Box 141, 57400 Thessaloniki, Greece*

[d] *IISER-Kolkata, Mohanpur Campus, Nadia 741252, India*

ARTICLE INFO

Article history:
Received 23 January 2012
Received in revised form
31 August 2012
Accepted 1 September 2012
Available online xxx

Keywords:
PEM fuel cell
Boost converter
Nonlinear stability analysis
Bifurcation
Chaos

ABSTRACT

The dynamical behaviour of a fuel cell feeding a boost converter is studied in this paper. A nonlinear model of the combined system is derived including the effect of the switching action of the converter. Using Filippov's theory, it is possible to analytically study the bifurcation patterns of the system and to demonstrate that the system loses stability through a period doubling bifurcation. To overcome this instability, we inject a high frequency sinusoidal signal into the system that forces the system to remain stable while at the same time retaining its basic slow scale properties (like the steady state error). This controller is simple to implement and does not require any special hardware. The stability analysis and new controller design method presented in this paper allow for the re-design of the converter to stabilize circuit operation with a substantially reduced inductor size, reducing the size and cost of the converter while maintaining its average currents and voltages and other circuit steady-state behaviour characteristics. The results are confirmed by using numerical and analytical tools.

1. Introduction

Fuel Cells (FCs) open a path to integrated energy systems since they are able to simultaneously address environmental challenges and major energy issues. FCs have received significant attention in the past 15 years and are expected to play an increasingly important role in future power generation facilities due to their flexibility to adapt to intermittent and diverse renewable energy sources. What's more, they are suitable for both stationary and mobile applications.

Existing categories of FC systems are mainly based on the type of electrolyte used and the operating conditions. In recent years there has been an increasing interest in utilizing Proton Exchange Membrane (PEM) FC systems for small portable, mobile or stationary applications. This type of FC is currently considered to be in a relatively more developed stage. PEMFCs utilize hydrogen and air to produce electricity

* *Corresponding author*. Chemical Process Engineering Research Institute (C.P.E.R.I.), Centre for Research and Technology Hellas (CE.R.T.H.), P.O. Box 60361, 57001 Thermi-Thessaloniki, Greece. Tel.: +30 2310 498 377; fax: +30 2310 498 380.
E-mail addresses: damian.giaouris@ncl.ac.uk, giaouris@cperi.certh.gr (D. Giaouris).

0360-3199/$ – see front matter Copyright © 2012, Hydrogen Energy Publications, LLC. Published by Elsevier Ltd. All rights reserved.
http://dx.doi.org/10.1016/j.ijhydene.2012.09.002

Nomenclature

A_{on}, B_{on}	State and input matrices during the on interval
A_{off}, B_{off}	State and input matrices during the off interval
a	Gain of high frequency injection controller
C	Boost converter capacitance, F
C_{Act}	Fuel cell capacitance, F
c_{O_2}	Oxygen concentration, mol/cm^3
D	Equilibrium of duty cycle
E	Eigenmatrix of the monodromy matrix
E_{Nerst}	Open circuit fuel cell voltage, V
f	General vector field
f_{on}, f_{off}	Vector fields
h	Scalar function of Σ
K_p, K_i	PI gains
k	Number of fuel cells
i_L	Output current of the fuel cell, A
I_{ref}	Steady state reference current, A
J_{on}, J_{off}	Jacobians of f_{off} and f_{on}
n	Normal vector of Σ
L	Boost converter inductance, H
R	Boost converter load, Ω
R_{Act}	Fuel cell activation losses, Ω
R_{Ohm}	Fuel cell Ohmic losses, Ω
S	Electronic switch
T	Switching period, s
T_e	FC temperature, K
t_k, $k \in \mathbb{N}$	Time instances, s
t_{on}	Interval where S is closed, s
V_{Act}	Activation voltage drop, V
V_{Cell}	Fuel cell output, V
V_{in}	Input voltage, V
V_{Ohm}	Ohmic voltage drop, V
V_{ref}	Demanded output voltage, V
v_c	Output voltage of boost converter, V
v_{ep}	Equilibrium of input voltage, V
x	State vector
x_0	Initial state vector
x_{ep}	Equilibrium of state vector
x_k, $k \in \mathbb{R}$	State variables

Greek symbols

δ	Small perturbation
Δi_L	Inductor current ripple, A
Δv_c	Output voltage ripple, V
$\Delta\phi$ (t, t_0, x_0)	Perturbation vector
Λ	Jordan canonical form of the monodromy matrix.
ξ_k, $k \in N$	Constants
Σ	Switching manifold
ϕ (t, t_0, x_0)	General solution
Φ (t, t_0)	State transition matrix
Φ ($T + t_0$, t_0)	Monodromy matrix
ψ	Angle of high frequency injection controller

and water. They have high power density, use solid electrolyte, have a long stack life and enjoy low degradation rates. The control of critical operating parameters such as the input flows of air and hydrogen, pressure and operating temperature, the management of water and the choice of the operating region lead to different characteristics for the system in terms of its profitability, effectiveness and safety.

In order to regulate the FC voltage output level, a power converter is necessary. Various converter topologies have been proposed depending on the application [1] with a boost converter being a popular choice [2]. The nonlinear behaviour of power converters has been extensively studied in numerous publications [3–5,13], which clearly demonstrate that the switching action required to step up the input voltage can cause various instabilities (called bifurcations) and can render the system behaviour unstable or even chaotic. More specifically, the switching action places a hyper-surface in the state space that forces the state trajectory to change when it crosses or touches this surface. This induces a number of nonlinear phenomena that are common to other nonlinear systems like period doubling bifurcations or the ones specific to nonsmooth systems like border collisions [5].

In this paper we study the interaction of these phenomena with the nonlinear behaviour of the FC which may cause the system to behave in an unpredictable or chaotic manner. This can have a direct effect on the life time of the FC as the resulting current ripple which increases when the converter becomes unstable, can damage the membranes of the FC [22]. In the past it was believed that the slow behaviour of the FC does not interact with the fast scale nonlinearities of the converter. However, it has been recently demonstrated [6,20] that it is possible for the voltage/current controlled boost converter to exhibit slow scale bifurcations [3] and these may interact with the slow scale dynamics of the FC.

As the industry demands more efficient systems with complicated multilevel and bidirectional power converters, it is imperative to study and understand these nonlinearities with the aim of avoiding them. The main goal of this paper is to provide the necessary tools to analytically study the combined system, to describe the nonlinear behaviour of the combined system, and to offer a robust but easy to implement control algorithm that guarantees a fast and stable response. Furthermore, we show that it is possible to reduce the inductance of the power converter by almost 50% using the proposed method, and still to have a stable system. This makes the system fast, light, cheap, and stable.

The paper is organized as follows: in Section 2 the system is described with emphasis on the boost converter and its basic properties. The full nonlinear model of the boost converter, the FC, the voltage PI controller and the current peak controller are derived in this section. In Section 3 we present briefly the stability analysis of its orbits, while in Section 4 we use the derived nonlinear and nonsmooth model with the aforementioned theory to analytically study the stability of the combined system. In the last section we propose a new supervising controller that stabilizes the system and this allows us to re-design the converter with a smaller inductance that can greatly improve the speed, cost, and weight of the combined system.

Please cite this article in press as: Giaouris D, et al., Nonlinear stability analysis and a new design methodology for a PEM fuel cell fed DC–DC boost converter, International Journal of Hydrogen Energy (2012), http://dx.doi.org/10.1016/j.ijhydene.2012.09.002

2. System description

2.1. Fuel cell

Typical characteristics of FC are normally expressed in the form of a polarization curve, which is a plot of cell voltage versus cell overall current density. To determine the voltage–current relationship of the cell, the cell voltage has to be defined as the difference between the ideal Nernst voltage and a number of voltage losses, which include the activation, Ohmic and concentration losses (which are ignored in this paper as we work in a region where they are negligible). The equation that takes into consideration the above voltage drops expresses [7] the output cell voltage as:

$$V_{Cell} = E_{Nernst} - V_{Act} - V_{Ohm} \quad (1)$$

where V_{Cell} is the FC output cell voltage, E_{Nerst} is the FC Open Circuit Voltage (OCV) and V_{Act}, V_{Ohm} are voltage drops that are functions of the current drawn from the FC.

Generally, the open circuit voltage depends on a number of factors like the temperature and the partial pressures of the gasses (air, H_2) but in this paper we assume that it is constant at 1.236 V [7], calculated at constant temperature and pressure conditions (65 °C, 1 Bar).

The activation drop is caused by the slowness of the reactions taking place on the surface of the electrodes. A part of the generated voltage is lost due to the chemical reaction that transfers the electrons to or from the electrodes. The activation losses are described by the Tafel equation [8]:

$$V_{Act} = \xi_1 + \xi_2 T_e + \xi_3 T_e \ln(i_L) + \xi_4 T_e \ln(c_{O_2}) \quad (2)$$

The form of (2) is considered to be a parametric equivalent of the general Butler–Volmer equation used to describe reaction kinetics at electrodes. This form has been derived from J.C. Amphlet et al. [21] and simplifies experimental validation by lumping all constant parameters of the fuel cell to ξ_i's. The only limitation of this equation is the fact that it is defined at all positive values of current in the operating range but not at zero current.

At some point, Ohmic and concentration losses prevail and the activation overvoltage is considered to be negligible at higher currents.

This description for the activation overvoltage takes into account the concentration of oxygen at the catalyst layer and various experimentally defined parametric coefficients.

At a later stage of the fuel cell operation, as current density rises, Ohmic voltage drops (V_{Ohm}) prevail. They are derived from the membrane resistance to the flow of electrons through the material of the electrodes and the various interconnections, as well as by the resistance to the flow of protons through the electrolyte:

$$V_{Ohm} = (\xi_5 + \xi_6 T + \xi_7 i_L) i_L \quad (3)$$

In the above equations ξ_k, ($k = 1\ldots7$) represent experimentally defined parametric coefficients whose values can vary from stack to stack. The values of these parameters used in this work are presented in Table 1 [7].

Table 1 – Parameters of the electrochemical model.

Electrochemical parameters	
Parameter	Value
$\xi_1, \xi_2, \xi_3, \xi_4$	1.3205, $-3.12\cdot10^{-3}$, $1.87\cdot10^{-4}$, $-7.4\cdot10^{-5}$
ξ_5, ξ_6, ξ_7	$3.3\cdot10^{-3}$, $-7.55\cdot10^{-6}$, $7.85\cdot10^{-4}$

The FC behaviour can also be modelled by an electrical equivalent circuit. This representation is based on the charge double layer phenomenon, which suggests that sudden changes in the current output of the FC do not imply sudden changes in its output voltage; instead there is a considerable time delay of a few seconds [9].

The resulting equivalent electric circuit of the FC is shown in Fig. 1 [9], where R_{Ohm} represents the Ohmic losses, R_{Act} the activation losses and C_{Act} is included to represent the double charge phenomenon. Using simple circuit theory techniques the equations for the activation and the Ohmic voltage drops are obtained:

$$R_{Act}(i_L) = \frac{V_{Act}}{i_L} = \frac{\xi_1 + \xi_2 T_e + \xi_3 T_e \ln(i_L) + \xi_4 T_e \ln(c_{O_2})}{i_L} \quad (4)$$

$$R_{Ohm}(i_L) = \frac{V_{Ohm}}{i_L} = \xi_5 + \xi_6 T_e + \xi_7 i_L \quad (5)$$

Experimentally, it has been observed that the capacitance C_{Act} is given by:

$$C_{Act}(i_L) = \frac{1}{3R_{Act}(i_L)} \quad (6)$$

Thus the nonlinear dynamical model that describes the FC is given by:

$$\frac{dV_{Act}}{dt} = \frac{1}{C_{Act}(i_L)}\left(i_L - \frac{V_{Act}}{R_{Act}(i_L)}\right) \quad (7)$$

Therefore the overall produced voltage is calculated as:

$$V_{Cell} = E_{nerst} - V_{Act} - i_L R_{Ohm}(i_L) \quad (8)$$

In order to assess the validity of the proposed model, a small-scale fully automated FC unit was used to generate experimental data under various conditions. The proposed model has been validated against experimental plant data

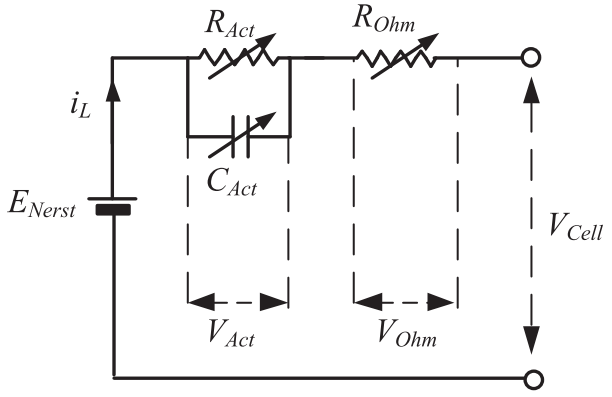

Fig. 1 – Fuel cell equivalent circuit allowing for the double charge phenomenon.

Please cite this article in press as: Giaouris D, et al., Nonlinear stability analysis and a new design methodology for a PEM fuel cell fed DC–DC boost converter, International Journal of Hydrogen Energy (2012), http://dx.doi.org/10.1016/j.ijhydene.2012.09.002

generated by the PEM fuel cell [7]. Fig. 2a illustrates the steady-state output of the model against the real behaviour of the FC. The graph shows that the model is reasonably accurate in the steady state. The voltage will slowly change as described by (6) and (7) during transients, i.e., when the FC current changes. If there is a step increase in current, the voltage will immediately drop (due to the term $i_L R_{Ohm}$) and then it will continue to decrease exponentially until it reaches a steady state (Fig. 2b). Both models (the one presented in [7] and the simplified one used here) showed exactly the same qualitative response with minor quantitative differences. For example when the current changes from 4 A to 6 A the model presented in [7] showed an immediate drop from 0.72 V to 0.68 V and after 2 s it converged to 0.6768 V while in the simple model the initial drop is from 0.71 V to 0.67 V and after 2 s it converged to 0.667 V.

As seen in Fig. 2, the single cell voltage is usually very small and FCs are therefore connected in series to achieve the desired output voltage. A series connection of cells is referred to as an FC stack and in this paper it is assumed that 30 single cells will make one FC stack giving an overall output voltage of:

$$V_{in}(t) = 30 \cdot V_{Cell}(t) \tag{9}$$

2.2. Boost converter

2.2.1. General description

The main function of a boost converter (Fig. 3) is to step-up the voltage produced by the FC stack. When the switch S is closed (for t_{on} s), the current i_L flows through the switch and the inductor L. Mathematically this is described [10,11] by the equation:

$$\frac{di_L}{dt} = \frac{1}{L} V_{in} \tag{10}$$

During the ON state, the inductor current will rise increasing the energy stored in the inductor:

$$E_L = \frac{1}{2} L i_L^2 \tag{11}$$

During this interval, the capacitor will discharge through the load reducing the capacitor voltage v_c:

$$\frac{dv_c}{dt} = -\frac{1}{RC} v_c \tag{12}$$

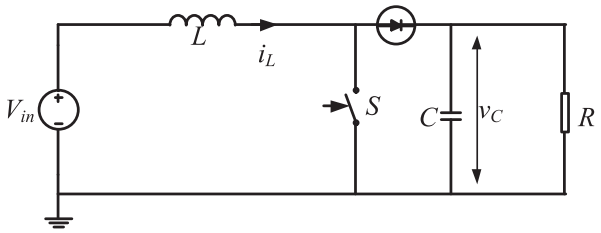

Fig. 3 – Schematic diagram of the boost converter.

When the switch is OFF (for t_{off} s), the energy stored in the inductor is delivered to the load while at the same time, charging the capacitor:

$$\frac{di_L}{dt} = \frac{1}{L}(V_{in} - v_c) \tag{13}$$

$$\frac{dv_c}{dt} = \frac{i_L R - v_c}{RC} \tag{14}$$

By repeating the above pattern periodically (at period T) it is possible to step up the input voltage to a required level. The ratio between t_{on} and T is the duty cycle d:

$$d = \frac{t_{on}}{T} \tag{15}$$

Assuming that the inductor current never falls to zero (a mode of converter operation referred to as continuous conduction mode or CCD), the relationship between the input and output voltage is given by:

$$\frac{v_c}{V_{in}} = \frac{1}{1-d} \tag{16}$$

Hence the overall state space model of the boost converter is given by the following piecewise smooth model:

$$\dot{x} = \begin{bmatrix} \dot{x}_1 \\ \dot{x}_2 \end{bmatrix} = \begin{cases} f_{on}, & \text{when S is on} : t \in [0, t_{on}] \\ f_{off}, & \text{when S is off} : t \in [t_{on}, T] \end{cases} \tag{17}$$

$$\text{where } f_{on} = \begin{bmatrix} \frac{-x_1}{RC} \\ \frac{V_{in}}{L} \end{bmatrix}, \quad f_{off} = \begin{bmatrix} \frac{x_2 R - x_1}{RC} \\ \frac{V_{in} - x_1}{L} \end{bmatrix},$$

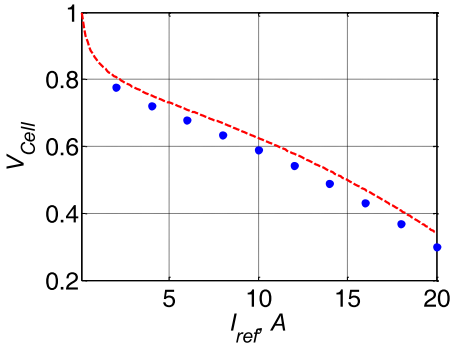

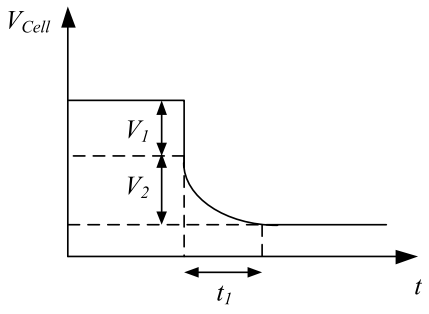

Fig. 2 – V–I curve of the FC, with red trace showing the results of the equivalent circuit; with the blue dots denoting the experimentally obtained results [7]. The curve was produced for fixed pressure and temperature conditions at 1 bar and 65 °C.

Please cite this article in press as: Giaouris D, et al., Nonlinear stability analysis and a new design methodology for a PEM fuel cell fed DC–DC boost converter, International Journal of Hydrogen Energy (2012), http://dx.doi.org/10.1016/j.ijhydene.2012.09.002

with x_1 being the output capacitor voltage and x_2 the inductor current.

Since the model of the converter is linear before and after the switching it can also be written as:

$$\dot{x} = \begin{cases} A_{on}x + B_{on}V_{in}, & S = \text{on} \\ A_{off}x + B_{off}V_{in}, & S = \text{off} \end{cases} \quad (18)$$

where

$$A_{on} = \begin{bmatrix} -\frac{1}{RC} & 0 \\ 0 & 0 \end{bmatrix}, \; A_{off} = \begin{bmatrix} -\frac{1}{RC} & \frac{1}{C} \\ -\frac{1}{L} & 0 \end{bmatrix}, \; B_{on} = B_{off} = \begin{bmatrix} 0 \\ \frac{1}{L} \end{bmatrix} \quad (19)$$

2.2.2. Conventional converter design

Conventional practice is for the parameters of the converter to be chosen based on a number of design specifications such as the desired switching frequency as well as an acceptable peak to peak current and voltage ripple content for a given application [10,11]. Higher switching frequencies result in smaller inductance and capacitance, better converter performance, but also in higher switching losses. The design process is inevitably a compromise. In this work the switching frequency was chosen to be 10 kHz. This is sufficient for our system as the FC time constant is of a few seconds. Other design criteria based on FC operational requirements were as follows:

1. Allowed current and voltage ripples of 0.4 pu and 0.1 pu, respectively
2. An operating duty cycle in the range 0.4–0.5 with V_{in} varying between 30 V and 36 V.
3. A load resistance of 50 Ohms.

Using the standard equations for a boost converter, the Voltage Ripple (VR) and Current Ripple (CR) contents are given by: $VR = T(V_{out} - V_{in}/RC)$ and $CR = (1/L)V_{in}DT$, giving design values of $L = 1.8$ mH, $C = 8$ μF.

In practice, these values are usually increased (with a direct adverse effect on the size and cost of the converter) to avoid the presence of subharmonics [3,12]. In this paper a supervising control law will be used instead to guarantee stable operation that does not require this size increment, thus reducing the size, weight and cost of the converter.

2.2.3. Control strategy and the average model of the boost converter

In order to study the system, a simple mathematical model that relates any changes to the duty cycle and input voltage to the output voltage and current is needed [10,11]. To derive this, the standard method of state space averaging (suitable for any piecewise smooth system) is normally employed. The average state space model is obtained by taking the average of the state and input matrices:

$$\dot{x} = (A_{on}d + A_{off}(1-d))x + (B_{on}d + B_{off}(1-d))V_{in}$$

$$\text{Or}: \quad \dot{x} = Ax + BV_{in} \quad (20)$$

$$\text{where } A = A_{on}d + A_{off}(1-d) = \begin{bmatrix} -\frac{1}{RC} & \frac{1}{C}(1-d) \\ -\frac{1}{L}(1-d) & 0 \end{bmatrix} \quad (21)$$

$$\text{and } B = B_{on}d + B_{off}(1-d) = \begin{bmatrix} 1 \\ \frac{1}{L} \end{bmatrix} \quad (22)$$

At the steady state, when the input voltage and duty cycle are v_{ep} and D respectively, the equilibrium state is:

$$\dot{x} = Ax + BV_{in} = 0 \Rightarrow x_{ep} = -A^{-1}Bv_{ep} \quad (23)$$

By making small changes to the duty cycle and input voltage we impose small variations on the state vector:

$$x = x_{ep} + \tilde{x}, \;\; v = v_{ep} + \tilde{v}, \;\; d = D + \tilde{d} \quad (24)$$

By substituting (24) into (19) and using (23) we get the linearised average state space equation that describes small perturbations around the equilibrium point:

$$\dot{\tilde{x}} = A\tilde{x} + B_v\tilde{v} + B_d\tilde{d} = A\tilde{x} + [B_d \quad B]\begin{bmatrix} \tilde{d} \\ \tilde{v} \end{bmatrix} \quad (25)$$

where $B_d = (A_{on} - A_{off})x_{ep} + (B_{on} - B_{off})v_{ep}$

Assuming that we observe both states, the overall transfer function is given by:

$$G(s) = (sI - A)^{-1}[B_d \quad B] = \frac{1}{s\left(s + \frac{1}{RC}\right) + \frac{1}{LC}(1-D)^2} \times \begin{bmatrix} -s\frac{v_{ep}}{RC(1-D)^2} + \frac{1}{C}\frac{v_{ep}}{L} & \frac{1}{LC}(1-D) \\ \frac{1}{L}\frac{v_{ep}}{RC(1-D)} + \left(s + \frac{1}{RC}\right)\frac{v_{ep}}{L(1-D)} & \frac{1}{L}\left(s + \frac{1}{RC}\right) \end{bmatrix} \quad (26)$$

Hence we deduce that the relationship between small changes in the duty cycle and the output voltage is:

$$G_{\tilde{v}_{out}\tilde{d}}(s) = \frac{\tilde{v}_{out}(s)}{\tilde{d}(s)} = v_{ep}\frac{-s\frac{1}{RC(1-D)^2} + \frac{1}{LC}}{s^2 + s\frac{1}{RC} + \frac{1}{LC}(1-D)^2} \quad (27)$$

In order to compensate for various disturbances and parameter variations, a closed loop control strategy is required. This means that the duty cycle will depend on the difference between the actual and demanded output voltage. However, we can see from (27) that there is a non-minimum phase zero in the transfer function between the duty cycle and the output voltage; for that reason an inner peak current control loop is added to improve the transient behaviour of the converter (Fig. 4).

In practical applications, the output voltage is measured through a high precision voltage divider, which in this work is modelled as a simple gain absorbed within the PI gains. A ramp compensator is added in the output of the PI controller to avoid the appearance of subharmonics in the system [14]. However, this adds a steady state error, which is considerable at high current ripple values. In the following sections, a new and more efficient method will be proposed that does not have this drawback, based on the stability analysis of the system presented in Section 3. Before the overall transfer function of the system can be derived, the inner current loop needs to be modelled. Fig. 5 [15], shows that a simple gain can represent the inner peak current control loop as follows:

Please cite this article in press as: Giaouris D, et al., Nonlinear stability analysis and a new design methodology for a PEM fuel cell fed DC–DC boost converter, International Journal of Hydrogen Energy (2012), http://dx.doi.org/10.1016/j.ijhydene.2012.09.002

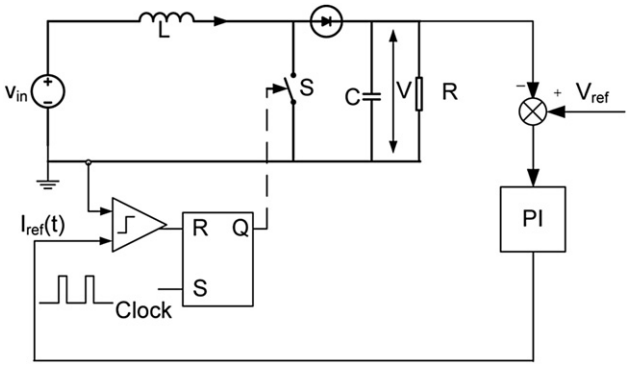

Fig. 4 – Current programmed boost converter.

$$T_m(s) = \frac{\tilde{d}(s)}{\tilde{i}_{ref}(s)} = \frac{D}{\Delta i_L} \tag{28}$$

Hence the overall transfer function is given by:

$$\frac{\tilde{v}_{out}(s)}{\tilde{v}_{ref}(s)} = G_{\tilde{v}_{out}\tilde{v}_{ref}}(s) = \frac{G_{\tilde{v}_{out}\tilde{i}_{ref}}(s)G_c(s)}{1 + G_{\tilde{v}_{out}\tilde{i}_{ref}}(s)G_c(s)} \tag{29}$$

where $G_c(s)$ is the PI controller transfer function given by:

$$G_c(s) = \frac{K_p s + K_i}{s} \tag{30a}$$

and the overall transfer function is:

$$G_{\tilde{v}_{out}\tilde{i}_{ref}}(s) = \frac{D}{\Delta i_L} v_{ep} \frac{-s\dfrac{1}{RC(1-D)^2} + \dfrac{1}{LC}}{s^2 + s\dfrac{1}{RC} + \dfrac{1}{LC}(1-D)^2} \tag{30b}$$

Using the previously determined converter parameter values and taking into account the effect of the peak current controller and the voltage divider while trying to avoid any wind-up problems or saturation of the duty cycle, the PI gains were chosen at $K_p = 0.01$, $K_i = 0.035$ giving a closed loop pole location at $10^3 \times (-0.62 \pm 6.09i)$ and -1.116; these values will ensure zero steady state error and good overall transient performance.

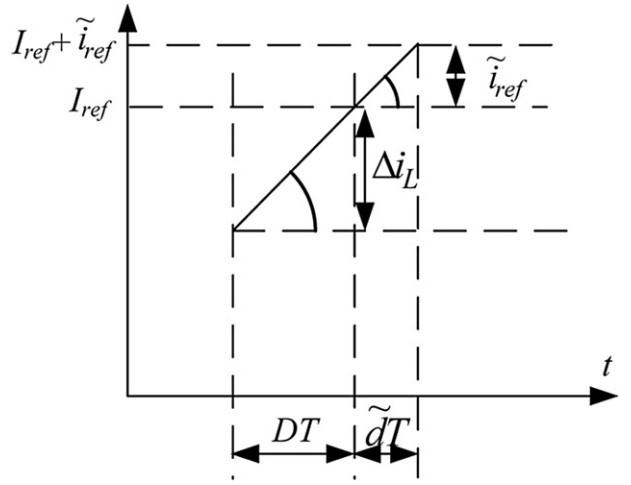

Fig. 5 – The effect of the inner peak current loop.

3. Proposed stability analysis method

3.1. Smooth orbits

In this section, basic stability analysis concepts are defined and extended to piece-wise smooth systems before the full nonlinear stability analysis of the boost converter including the FC and the PI controller is presented and validated in Section 4, using both analytical and numerical tools.

If we assume that we have a generic initial value problem:

$$\frac{dx(t)}{dt} = f(x(t), t), \quad x(t_0) = x_0 \tag{31}$$

then, according to Poincaré, the stability of a specific solution $\phi(t, t_0, x_0)$ can be tested by adding a small perturbation, i.e. $x(t_0) = x_0 + \delta$ and then monitoring the evolution of the perturbation vector:

$$\frac{d}{dt}\Delta\phi(t, t_0, x_0) = \left.\frac{\partial f(x(t), t)}{\partial x(t)}\right|_{x(t)=\phi(t,t_0,x_0)} \Delta\phi(t, t_0, x_0) \tag{32}$$

where $\Delta\phi(t, t_0, x_0) = \phi(t, t_0, x_0 + \delta) - \phi(t, t_0, x_0)$. The orbit is called stable (with respect to some norm) if the perturbed orbit remains "close" to the original one. The solution of (32) is given by:

$$\Delta\phi(t, t_0, x_0) = \frac{\partial\phi(t, t_0, x_0)}{\partial x_0}\Delta\phi(t_0, t_0, x_0) = \Phi(t, t_0)\Delta\phi(t_0, t_0, x_0) \tag{33}$$

where $\Phi(t_0, t_0)$ is the state transition matrix of (32) with the property that $\Phi(t_0, t_0) = I$. (34)

Practically the orbit is stable when the limit of the perturbation vector tends to zero as $t \to \infty$.

In order to find the state transition matrix $\Phi(t, t_0)$ we have to use the fundamental theorem of calculus and consider the original vector field:

$$\phi(t, t_0, x_0) = x_0 + \int_{\tau=t_0}^{\tau=t} f(\phi(\tau, t_0, x_0), \tau)d\tau \tag{35}$$

By differentiating with respect to x_0 and then with respect to t we get (36), which is a matrix differential equation that can be solved to determine $\Phi(t,t_0)$:

$$\frac{\partial\phi(t, t_0, x_0)}{\partial x_0} = I + \int_{\tau=t_0}^{\tau=t} \frac{\partial f(\phi(\tau, t_0, x_0), \tau)}{\partial\phi(\tau, t_0, x_0)} \frac{\partial\phi(\tau, t_0, x_0)}{\partial x_0} d\tau \tag{36}$$

$$\frac{d}{dt}\left(\frac{\partial\phi(t, t_0, x_0)}{\partial x_0}\right) = \left.\frac{\partial f(x(t), t)}{\partial x(t)}\right|_{x(t)=\phi(t,t_0,x_0)} \frac{\partial\phi(t, t_0, x_0)}{\partial x_0} \tag{37}$$

If $\phi(t, t_0, x_0)$ is a periodic orbit of period T, then it can be proved [16] that:

$$\Delta\phi(kT + t_0, t_0, x_0) = \Phi^k(T + t_0, t_0)\Delta\phi(t_0, t_0, x_0) \tag{38}$$

where $\Phi(T + t_0, t_0)$ is the monodromy matrix of the periodic orbit. Thus, the monodromy matrix is nothing but the state transition matrix over a whole period T.

By using the Jordan canonical form $\Lambda(t)$ of the Modoromy matrix, (37) can be written as:

Please cite this article in press as: Giaouris D, et al., Nonlinear stability analysis and a new design methodology for a PEM fuel cell fed DC–DC boost converter, International Journal of Hydrogen Energy (2012), http://dx.doi.org/10.1016/j.ijhydene.2012.09.002

$$\Delta\phi(kT + t_0, t_0, x_0) = E\Lambda^k(t)E^{-1}\Delta\phi(t_0, t_0, x_0) \quad (39)$$

where E is the eigenmatrix of the Monodromy matrix.

From (38) is it clear that if the eigenvalues of the monodromy matrix (also called the Floquet multipliers) have magnitudes less than 1, then the periodic orbit is stable [17].

There are 3 basic scenarios where the periodic orbit losses stability [5,17], depending on the location of the Floquet multipliers:

1. One eigenvalue becomes 1; this is referred to as a saddle node bifurcation.
2. One eigenvalue becomes −1; this is referred to as a period doubling bifurcation.
3. Two complex eigenvalues cross the unit circle; this is referred to as a Neimark–Sacker bifurcation.

3.2. Nonsmooth orbits

The aforementioned methodology cannot be directly applied to our system as its vector field is piecewise smooth and hence (35) does not hold. To better understand this issue assume the scenario depicted in Fig. 6, where a two dimensional state space is divided into two areas through a surface Σ (called the switching manifold):

$$\mathbb{R}^2 = V_- \cup \Sigma \cup V_+ \quad (40)$$

In the area V_- the system is described by $f_1(x(t), t)$ and in V_+ by $f_2(x(t), t)$:

$$\dot{x}(t) = \begin{cases} f_1(x(t), t) & x \in V_- \\ f_2(x(t), t) & x \in V_+ \end{cases} \quad (41)$$

The surface Σ is defined by a scalar function $h(x(t), t)$ and the normal vector to Σ is:

$$n = \nabla h(x(t), t) \quad (42)$$

For simplicity, we assume in this work that at the point of switching there is no jump in the state vector (these systems are called Filippov systems or systems with degree of smoothness 1 [5,18]). If we assume that at $t = t_0$, we have an orbit that starts from the point $x_0 \in V_-$, and at $t_1 = t_\Sigma$ crosses the switching surface at the point $x_\Sigma \in \Sigma$, before it continues into V_+. To study the stability of this orbit we add a perturbation at x_0 and we observe the perturbation vectors. The perturbed orbit crosses Σ at $t_2 = t_1 + \Delta t$, where Δt may be positive or negative but most likely it is going to be nonzero. In this paper and without loss of generality we assume that it is positive, i.e. the new orbit crosses the switching manifold at a later instant than the original one. As with the smooth case, we need to model the perturbation vectors but the analysis breaks down during the interval $[t_1, t_2]$ (it has to be noted that this small interval depends on the initial point x_0 and on the initial perturbation δ). Mathematically the orbit at the point x_Σ is not differentiable with respect to x. There are several ways to overcome this problem including the discontinuity map method [5], but in this paper we follow the methodology proposed by Filippov [16–18] where the perturbation vector at $t = t_1$ is mapped to the perturbation vector at $t = t_2$. This map is called the Saltation or jump matrix and is derived using a local approximation of the orbits and the surface Σ near the point of switching [16]:

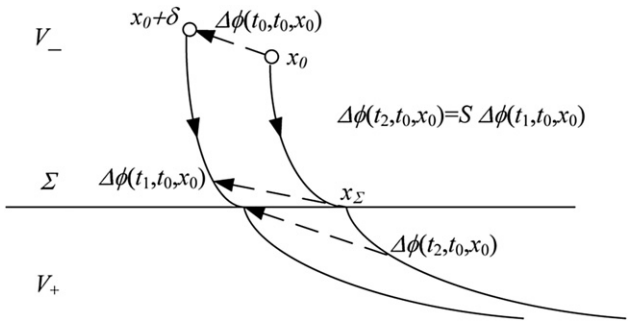

Fig. 6 – Concept of the saltation matrix.

$$\Delta\phi(t_2, t_0, x_0) = S\Delta\phi(t_1, t_0, x_0) \quad (43)$$

$$\text{where } S = I + \frac{\left(\lim_{t\to t_\Sigma^-} f_1(x(t), t) - \lim_{t\to t_\Sigma^+} f_2(x(t), t)\right) n^T}{n^T \lim_{t\to t_\Sigma^+} f_2(x(t), t) + \left.\frac{\partial h(x(t), t)}{\partial t}\right|_{t=t\Sigma}} \quad (44)$$

Hence the monodromy matrix is given by:

$$\Phi(t_0 + T, t_0) = \Phi(t_0 + T, t_\Sigma)\cdot S \cdot \Phi(t_\Sigma, t_0) \quad (45)$$

$$\text{where } \Phi(t_0 + T, t_\Sigma) = \frac{\partial\phi(t, t_\Sigma, x_\Sigma)}{\partial x_\Sigma} \text{ and } \Phi(t_\Sigma, t_0) = \frac{\partial\phi(t, t_0, x_0)}{\partial x_0} \quad (46)$$

Unfortunately, in most cases we cannot find the two state transition matrices given in (46) in closed form (unless the vector fields before and after the switching are linear [12]) and hence we have to use numerical methods. In both cases we have to use (37) which means that we need to find the Jacobian matrices of the two vector fields evaluated along the orbit. These two Jacobian matrices are numerically calculated from (37) using Maple for the intervals before and after the switching, taking into account that a state transition matrix is the identity matrix at the beginning of each interval. In this paper, a brute force numerical approach is used and hence these two Jacobian matrices can be calculated only when the orbit is stable, by simulating the system for one clock cycle and using the numerical values of the state vector in (37) and (44). As a parameter changes and the orbit becomes less stable, i.e. we get closer to a bifurcation point; the Floquet multipliers approach the unit circle. Alternately the method first presented in [19] by one of the co-authors of the paper could have been used.

4. Stability analysis of the overall system

In this section we will use the previously outlined analysis to determine the stability of the overall system. The mathematical model of the system is of 4th order, with 2 states (x_1, x_2) representing the boost converter (18) and (19), one state (x_3) the FC (7) and (8) and another state (x_4) the output of the integrator in the external PI controller (30a). Hence the vector fields before and after the switching are:

$$f_{on}=\begin{bmatrix}\dfrac{-x_1}{RC}\\ \dfrac{k(E-x_3-x_2R_r)}{L}\\ \dfrac{1}{C_{Act}(x_2)}\left(x_2-\dfrac{x_3}{R_{Act}(x_2)}\right)\\ V_{ref}-x_1\end{bmatrix} \text{ and} \tag{47}$$

$$f_{off}=\begin{bmatrix}\dfrac{x_2R-x_1}{RC}\\ \dfrac{k(E-x_3-x_2R_r)-x_1}{L}\\ \dfrac{1}{C_{Act}(x_2)}\left(x_2-\dfrac{x_3}{R_{Act}(x_2)}\right)\\ V_{ref}-x_1\end{bmatrix}$$

The switching manifold is given by the scalar equation:

$$\begin{aligned}h(x(t),t)=&x_2-I_{ref}=x_2-\left(K_pe+K_i\int e\,dt\right)\\ &=x_2-\left(K_p(V_{ref}-x_1)+K_i\int V_{ref}-x_1\,dt\right)\Rightarrow h(x(t),t)\\ &=x_2-K_pV_{ref}+K_px_1-K_ix_4\end{aligned} \tag{48}$$

Thus the normal vector is given by

$$n=\begin{bmatrix}K_p & 1 & 0 & -K_i\end{bmatrix}^T \tag{49}$$

And the saltation matrix is:

$$S=I+\begin{bmatrix}K_p\dfrac{x_2R}{RC} & \dfrac{x_2R}{RC} & 0 & -K_I\dfrac{x_2R}{RC}\\ \dfrac{-K_px_1}{L} & \dfrac{-x_1}{L} & 0 & \dfrac{K_Ix_1}{L}\\ 0 & 0 & 0 & 0\\ 0 & 0 & 0 & 0\end{bmatrix}\times\left(K_p\frac{-x_1}{RC}+\frac{k(E-x_3-x_2R_r)}{L}-K_I(V_{ref}-x_1)\right) \tag{50}$$

The two Jacobians are found to be:

$$J_{off}=\begin{bmatrix}-\dfrac{1}{RC} & \dfrac{1}{C} & 0 & 0\\ -\dfrac{1}{L} & -\dfrac{k(\xi_5+\xi_6T+2\xi_7x_2)}{L} & -\dfrac{30}{L} & 0\\ 0 & \dfrac{3\xi_3T}{x_2} & -3 & 0\\ -1 & 0 & 0 & 0\end{bmatrix} \tag{51}$$

$$J_{on}=\begin{bmatrix}-\dfrac{1}{RC} & 0 & 0 & 0\\ 0 & -\dfrac{k(\xi_5+\xi_6T+2\xi_7x_2)}{L} & -\dfrac{30}{L} & 0\\ 0 & \dfrac{3\xi_3T}{x_2} & -3 & 0\\ -1 & 0 & 0 & 0\end{bmatrix} \tag{52}$$

In this paper the demanded voltage V_{ref} is chosen as the bifurcation variable. The results of the analysis are summarised in Table 2, where we can clearly see that as we approach a demanded output voltage of 40.1 V there is a period doubling bifurcation since one of the Floquet multipliers tends to −1. Two eigenvalues are close to 1 (to four decimal places) because of the presence of the slow outer PI controller & FC dynamics (compared to the boost converter). To further validate this result the bifurcation diagram of the system was computed (Fig. 7) clearly showing a period doubling bifurcation just after 40.1 V. This is further confirmed by the numerical time domain results presented in Fig. 8.

Table 2 – Results of the combined system FC/Converter.

V_{ref}, V	Floquet multipliers of the period 1 orbit			
39	−0.929	0.2506	1.000	0.9997
40	−0.9913	0.2644	1.000	0.9997
40.1	−0.999	0.2644	1.000	0.9997

The subharmonics that appear in Fig. 8 can greatly downgrade the system's performance. The presence of subharmonics may reduce the FC's life time [2], will decrease the efficiency of the converter due to the presence of extra AC components. If the bifurcations result in a chaotic orbit then the ripple will be larger (hence larger losses), the spectrum will be spread (hence the filter would be ineffective), and it will be highly uncontrollable (due to the sensitive dependence on the initial conditions).

5. Efficient design method

It has been mentioned earlier that once a power electronics practitioner determines the required values of the LC filter based on some chosen design criteria, he/she has to oversize the filter in order to avoid the subharmonic instability depicted in Fig. 7. Another complementary approach is to use a ramp compensator, which has the negative result of increasing the steady state error, in addition to the fact that it cannot be applied to any other converter apart from a boost converter with a current loop. In this section, a new supervising control law will be proposed that guarantees a wide stable operating range and zero steady state error while simultaneously offering the possibility of reducing the size of the circuit inductance, an extremely important consideration for example in electric vehicle applications where size, weight

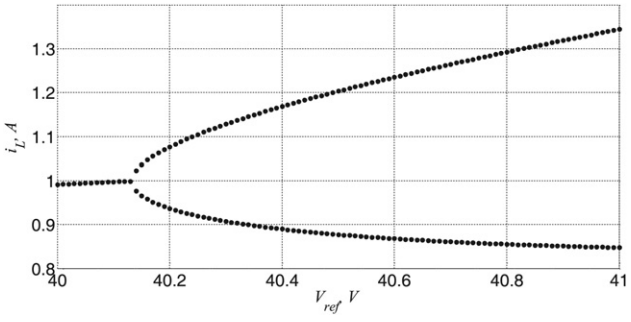

Fig. 7 – Bifurcation diagram.

Please cite this article in press as: Giaouris D, et al., Nonlinear stability analysis and a new design methodology for a PEM fuel cell fed DC–DC boost converter, International Journal of Hydrogen Energy (2012), http://dx.doi.org/10.1016/j.ijhydene.2012.09.002

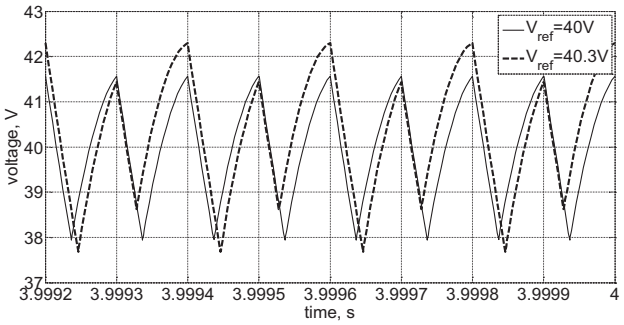

Fig. 8 – Steady state output voltage for $V_{ref} = 40$ and 40.3 V.

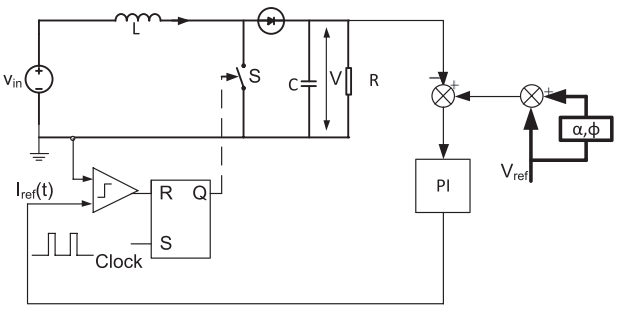

Fig. 10 – Supervising controller.

and the cost factors are of paramount importance. This method can easily be applied to any converter.

The new design process is based on the concept of making small changes to the Saltation matrix that will not change the location of the limit cycle (i.e. will not add a steady state error) but will change the stability properties of the system. From (44) we see that altering the time derivative of the scalar equation that describes the switching manifold can influence the Saltation matrix:

$$S = I + \frac{\left(\lim_{t\to t_\Sigma^-} f_1(x(t),t) - \lim_{t\to t_\Sigma^+} f_2(x(t),t)\right) n^T}{n^T \lim_{t\to t_\Sigma^+} f_2(x(t),t) + \left.\frac{\partial h(x(t),t)}{\partial t}\right|_{t=t\Sigma}} \tag{53}$$

Thus if the demanded voltage changes from V_{ref} to $V_{ref}(1 + a \sin(\omega t + \psi))$ the scalar function h will become:

$$h(x(t),t) = x_2 - K_p V_{ref}(1 + a\sin(\omega t + \psi)) + K_p x_1 - K_i x_4$$

And hence the time derivative will change from zero to:

$$\frac{\partial h(x(t),t)}{\partial t} = -K_p V_{ref} a\omega \cos(\omega t + \psi) \tag{54}$$

where the frequency ω is equal to the clock frequency.

The phase shift ψ is chosen such that $\sin(\omega\, dT + \psi) = 0$ implying that the switching will take place at the same instant and at the same location in state space as the original orbit. It is very easy to determine the duty cycle as the demanded voltage (we assume that the steady state error is zero) and the input voltage (from the V–I curve) are known. Thus, in the above scenario, the duty cycle is given by:

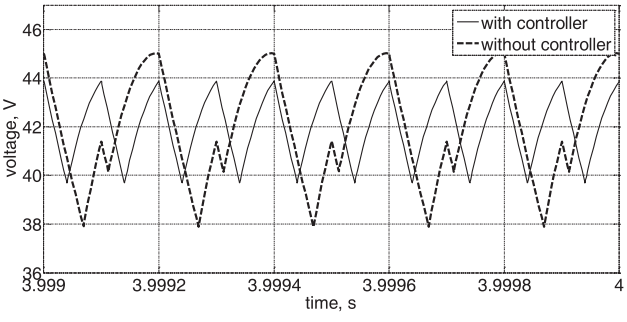

Fig. 9 – Steady state output voltage for $V_{ref} = 42$ with and without the supervising control law.

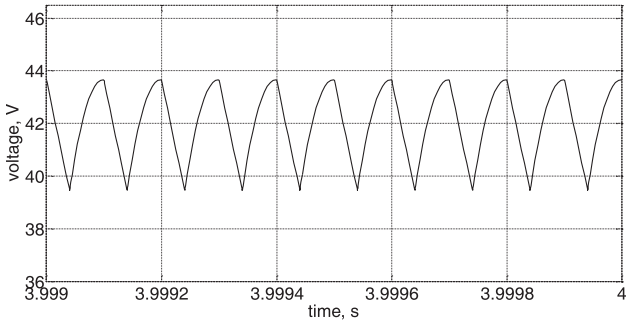

Fig. 11 – Steady state output voltage for $V_{ref} = 42$ and $L = 0.9$ mH with the supervising control law.

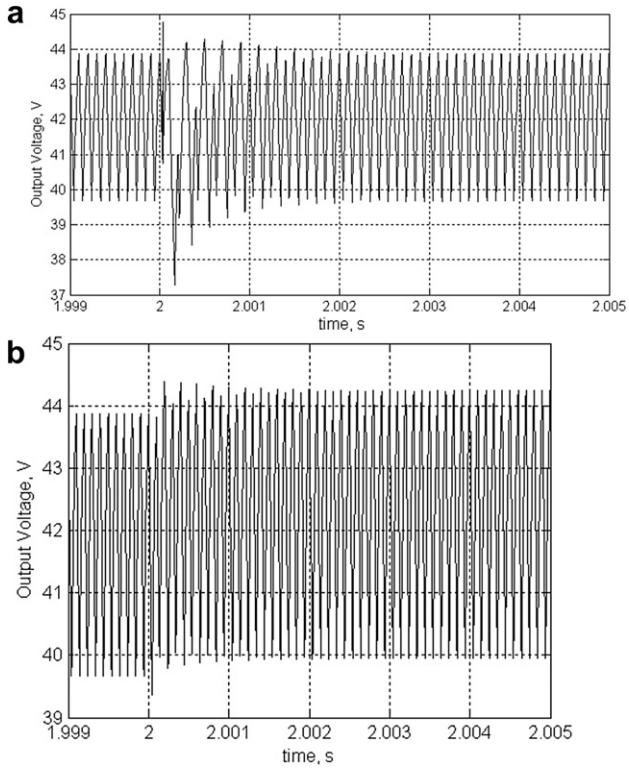

Fig. 12 – Responses of the controlled system for a) a 10% state perturbation and a step increase of the demanded output voltage from 42 V to 43 V.

Please cite this article in press as: Giaouris D, et al., Nonlinear stability analysis and a new design methodology for a PEM fuel cell fed DC–DC boost converter, International Journal of Hydrogen Energy (2012), http://dx.doi.org/10.1016/j.ijhydene.2012.09.002

Table 3 – Results of the system using the supervising controller, $L = 1.8$ mH, $V_{ref} = 42$ V.

a	Floquet multipliers of the period 1 orbit			
−0.5	−0.8495	0.2328	1.000	0.9997
−0.8	−0.7064	0.2070	1.000	0.9997
−2	$\lvert -0.0671 + 0.1029i \rvert = 0.1228$		1.000	0.9997

$$d = \frac{V_{out} - V_{in}}{V_{out}} = \frac{V_{ref} - V_{in}}{V_{ref}} = \frac{42 - 25}{42} \approx 0.4 \tag{55}$$

Hence $\sin(2\pi 0.4 + \psi) = 0 \Rightarrow \psi = -0.8\pi$

The value of a can be obtained using a numerical method [12] or by trial and error. For example, if we choose $a = -0.5$ the previously unstable period one orbit becomes stable again as shown in Fig. 9. Thus we propose the use of a supervising controller (Fig. 10) that will change the values of a and ψ depending on the demanded voltage in such a way as to force the period one orbit to remain stable. Moreover, the stable orbit shown in Fig. 9 shows a smaller ripple content than that the original stable orbit. Hence it is possible to decrease the value (and hence the size, weight and cost) of the inductance and still have a stable system using the above controller. This is demonstrated in Fig. 11 where the inductance value is halved (Fig. 10).

Two more tests were conducted to validate the aforementioned controller. In the first test the demanded signal was increased from 42 V to 43 V and in the second test a perturbation was added once the system had reached its steady state, Fig. 12. Both tests show that the orbit is stable. In order to quantify the stability of the controlled system, we calculated the Floquet multipliers using the method described in [6]. For a larger absolute value of the control signal (variable "a") the absolute values of the Floquet Multipliers become smaller indicating a more stable system. The results are summarised in Tables 3 and 4.

6. Conclusions

The nonlinear behaviour of a voltage/current controlled boost converter fed by a FC has been studied in this paper, clearly showing how the system can lose stability through a period doubling bifurcation. The FC was modelled using a nonlinear, current dependent RC equivalent circuit and its output was fed to a conventional PI controlled boost converter with current-mode control. A boost converter was designed based on standard ripple criteria and its state space averaging model was derived including the outer PI and the inner peak controllers. Thus the study was based on the full nonlinear model of the combined system based on differential equations. In order to determine the stability of the combined system, Floquet theory was used in conjunction with Filippov's method to model the behaviour of the system during the switching events. The eigenvalues of the monodromy matrix were used to determine the stability of the nominal periodic motion. It was shown that the converter loses stability as the reference voltage increases; for example, for the choice of parameters used in this paper the converter becomes unstable at $V_{ref} \approx 40.1$ V. This analysis showed for the first time that under nominal conditions there are quantitative differences of the stability properties of the converter when it is fed either by a constant supply and or an FC, though the bifurcation scenarios are qualitatively similar.

Finally a new supervising control law is proposed in this paper that both stabilises the overall system (FC and converter) and allows us to reduce the converter inductance by as much as 50%, thus making the system faster making the system faster, lighter and less expensive. This allows for a new and more efficient design of the converter that will make the use of FC more attractive in various applications like electric vehicles.

Table 4 – Results of the system using the supervising controller, $L = 0.9$ mH, $V_{ref} = 42$ V.

a	Floquet multipliers of the period 1 orbit			
−0.5	−0.9495	0.3038	1.000	0.9997
−0.8	−0.8897	0.2943	1.000	0.9997
−2	−0.6686	0.2512	1.000	0.9997

Acknowledgments

This work is co-financed by the National Strategic Reference Framework (NSRF) 2007–2013 of Greece and the European Union, research program "Archimedes III" (OPT-VIPS).

REFERENCES

[1] Emadi A, Williamson SS, Khaligh A. Power electronics intensive solutions for advanced electric, hybrid electric, and fuel cell vehicular power systems. IEEE Transactions on Power Electronics 2006;21(3):567–77.
[2] Fontes G, Turpin C, Astier S, Meynard TA. Interactions between fuel cells and power converters: influence of current harmonics on a fuel cell stack. IEEE Transactions on Power Electronics 2007;22(2):670–8.
[3] Banerjee S, Verghese GC. Nonlinear phenomena in power electronics: attractors, bifurcations chaos, and nonlinear control. New York: IEEE Press; 2001.
[4] Tse CK. Complex behavior of switching power converters. Boca Raton, FL: CRC; 2003.
[5] di Bernardo M, Budd C, Champneys AR, Kowalczyk P. Piecewise-smooth dynamical systems. London, U.K: Springer-Verlag; 2008.
[6] Giaouris D, Banerjee S, Imrayed O, Mandal K, Zahawi B, Pickert V. Complex interaction between tori and onset of three-frequency quasi-periodicity in a current mode controlled boost converter. IEEE Transactions on Circuits and Systems I: Regular Papers 2012;59(1):207–14.
[7] Ziogou C, Voutetakis S, Papadopoulou S, Georgiadis M. Modelling and experimental validation of a PEM fuel cell system. Computers and Chemical Engineering 2011;35(9):1886–900.
[8] Mann R. Development and application of a generalised steady-state electrochemical model for a PEM fuel cell. Journal of Power Sources 2000;86(1–2):173–80.
[9] Larminie J, Dicks A. Fuel cell systems explained. Wiley; 2003.

Please cite this article in press as: Giaouris D, et al., Nonlinear stability analysis and a new design methodology for a PEM fuel cell fed DC–DC boost converter, International Journal of Hydrogen Energy (2012), http://dx.doi.org/10.1016/j.ijhydene.2012.09.002

[10] Erickson RW, Maksimovic D. Fundamentals of power electronics. USA: Springer; 2001.
[11] Kassakian JG, Schlecht MF, Verghese GC. Principles of power electronics. Reading MA: Addison-Wesley; 1991.
[12] Giaouris D, Banerjee S, Zahawi B, Pickert V. Stability analysis of the continuous-conduction-mode buck converter via Filippov's method. IEEE Transactions on Circuits and Systems – I 2008;55(4):1084–96.
[13] Di Bernardo M, Vasca F. Discrete-time maps for the analysis of bifurcations and chaos in dc/dc converters. IEEE Transactions on Circuits and Systems – I, Fundamental Theory Applications 2000;47(2):130–43.
[14] Forsyth AJ, Mollov SV. Modelling and control of DC–DC converters. Power Engineering Journal 1998;12(5):229–36.
[15] Kazimierczuk MK. Transfer function of current modulator in PWM converters with current-mode control. IEEE Transactions on Circuits and Systems – I, Fundamental Theory Applications 2000;47(9):1407–12.
[16] Leine RI, Nijmeijer H. Dynamics and bifurcations of non-smooth mechanical systems. Berlin: Springer-Verlag; 2004.
[17] Kuznetsov YA. Elements of applied bifurcation theory. New York: Springer-Verlag; 2004.
[18] Filippov AF. Differential equations with discontinuous righthand sides. Dordrecht, The Netherlands: Kluwer; 1988.
[19] Mandal K, Banerjee S, Chakraborty C. Symmetry-breaking bifurcation in load resonant dc-dc converters. In: IEEE international symposium on circuits and systems (ISCAS), Brazil; 15–18 May 2011. p. 1327–30.
[20] Banerjee S, Giaouris D, Missailidis P, Imrayed O. Local bifurcations of a quasiperiodic orbit. Accepted for publication at International Journal of Bifurcation and Chaos.
[21] Amphlett JC, Baumert RM, Mann RF, Peppley BA, Roberge RP, Harris TJ. Performance modelling of the Ballard Mark IV solid polymer electrolyte fuel cell I. Mechanistic model development. Journal of Electrochemical Society 1995;142(1):1–8.
[22] Choi W, Joung G, Enjeti P, Howze J. An experimental evaluation of the effects of ripple current generated by the power conditioning stage on a proton exchange membrane fuel cell stack. Journal of Power Sources June 2004;13(3): 257–64.

Please cite this article in press as: Giaouris D, et al., Nonlinear stability analysis and a new design methodology for a PEM fuel cell fed DC–DC boost converter, International Journal of Hydrogen Energy (2012), http://dx.doi.org/10.1016/j.ijhydene.2012.09.002